Lehrstuhl für Bildverarbeitung
Institute of Imaging & Computer Vision

New Criteria for Shift Variance and Wide-Sense Cyclostationarity in Multirate Filter Banks

Til Aach

Institute of Imaging and Computer Vision
RWTH Aachen University, 52056 Aachen, Germany
tel: +49 241 80 27860, fax: +49 241 80 22200
web: www.lfb.rwth-aachen.de

in: International Workshop on Spectral Methods and Multirate Signal Processing (SMMSP).
See also BibTeX entry below.

BibTeX:

```
@inproceedings{AAC06a,
author = {Til Aach},
title = {New Criteria for Shift Variance and Wide-Sense Cyclostationarity
                          in Multirate Filter Banks},
booktitle = {International Workshop on Spectral Methods and Multirate Signal
                          Processing (SMMSP)},
editor = {T. Saram\"aki and K. Egiazarian and J. Astola},
publisher = {TICSP Series, ISBN: 952-15-1624-0},
address = {Florence},
month = {Sept.\ 2 -- 3},
year = {2006},
pages = {7--13 (also on CD-ROM)}}
```


document created on: October 13, 2006
created from file: aac06a_cover.tex
cover page automatically created with CoverPage.sty
(available at your favourite CTAN mirror)

RWTH AACHEN
RHEINISCH-WESTFÄLISCHE TECHNISCHE HOCHSCHULE AACHEN

NEW CRITERIA FOR SHIFT VARIANCE AND WIDE-SENSE CYCLOSTATIONARITY IN MULTIRATE FILTER BANKS

Til Aach

Institute of Imaging and Computer Vision, RWTH Aachen University,
D-52056 Aachen, Germany, til.aach@lfb.rwth-aachen.de

ABSTRACT

Sampling rate conversion in multirate filter banks leads to time-varying phenomena, which differ between deterministic and stationary random signals. More specifically, downsampling causes deterministic signals to become periodically shift variant, while upsampling turns stationary random signals into cyclostationary signals. We provide criteria for the quantification of these effects, and compare a variety of paraunitary and biorthogonal perfect reconstruction filter banks as well as orthogonal block transforms. Our criteria also permit frequency-resolved evaluations.

1. INTRODUCTION

Downsampling and upsampling in multirate filter banks generates time-dependent phenomena, the descriptions of which differ depending on whether the signals are viewed as deterministic or wide sense stationary (WSS) [1, 2, 3, 4, 5, 6, 7, 8, 9]. Based an earlier comparative analysis of these effects [10, 11], we develop here criteria to quantify the shift variance and cyclostationarity generated. While in [10, 11], we have only quantified periodic shift variance of subband energies for deterministic signals, and the cyclic nonstationary behaviour of subband powers for random signals, we extend our analysis here towards energy *spectra* and power *spectra*. Besides giving scalar numerical quantities for the evaluation of shift variance and cyclic nonstationarity, our criteria also enable the analysis over frequency or individual subbands.

2. DETERMINISTIC AND RANDOM SIGNALS IN MULTIRATE FILTER BRANCHES

Figure 1 shows one branch of a multirate filter bank, consisting of analysis and synthesis filters $H(z)$ and $G(z)$, and of a downsampler followed by an upsampler. In the following, we first describe the effects of decimation and interpolation on the energy spectra and power spectra of deterministic and WSS signals, respectively. We then develop our criteria, and apply these to a variety of widely-used paraunitary and biorthogonal perfect reconstruction (PR) filter banks, and to three orthogonal block transforms, viz. DCT, MLT and LOT. The input signal is denoted as $s(n)$. In the deterministic case, it is assumed to be of finite energy with z-transform $S(z)$ and energy spectrum $R^E_{ss}(z) = S(z)S(z^{-1})$. In the WSS case, its autocorrelation function (ACF) is $r_{ss}(n)$, and its power spectrum is $R_{ss}(z)$. The Mth root of one is denoted by $e^{-j2\pi/M} = W$, and the Fourier matrix by $\mathbf{W}$. The modulation vector of a signal $s(n)$ is denoted by $\mathbf{s}_m(z) = [S(z), S(zW), \ldots, S(zW^{M-1})]^T$.

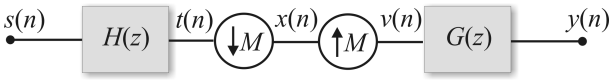

Figure 1. One branch of a multirate filter bank, consisting of an analysis filter $H(z)$ followed by a downsampler of factor M. The synthesis part consists of an upsampler and an interpolation filter.

2.1. Decimation

2.1.1. Deterministic Signals

Downsampling of the analysis-filtered signal $t(n) \circ\!-\!\bullet\, T(z) = H(z)S(z)$ yields

$$X(z) = 1/M \cdot \mathbf{s}_m^T(z^{1/M}) \cdot \mathbf{h}_m(z^{1/M}) \qquad (1)$$

and, for the energy spectrum

$$\begin{aligned} R^E_{xx}(z) &= X(z)X(z^{-1}) \qquad (2)\\ &= \frac{1}{M^2}\mathbf{s}_m^T(z^{1/M})\mathbf{R}^E_{hh}(z^{1/M})\mathbf{s}_m(z^{-1/M}) \end{aligned}$$

with the $M \times M$-matrix $\mathbf{R}^E_{hh}(z)$ given by $\mathbf{R}^E_{hh}(z) = \mathbf{h}_m(z) \cdot \mathbf{h}_m^T(z^{-1})$. When the signal $s(n)$ is shifted by m samples to $s(n-m)$, $m = 0, \ldots, M-1$, $T(z)$ is multiplied by the phase term z^{-m}, and the energy spectrum $R^E_{xx}(m,z)$ becomes

$$\begin{aligned} R^E_{xx}(m,z) = \quad & \tfrac{1}{M} \sum_{k=0}^{M-1} T(z^{\frac{1}{M}}W^k) \cdot W^{-km} \cdot \\ & \tfrac{1}{M} \sum_{l=0}^{M-1} T(z^{-\frac{1}{M}}W^l) \cdot W^{-lm} \qquad (3) \end{aligned}$$

which generally depends on the shift m. Assembling $R^E_{xx}(m,z)$ for $m = 0, \ldots, M-1$ into a vector yields

$$\begin{aligned} &\left[R^E_{xx}(0,z), R^E_{xx}(1,z), \ldots, R^E_{xx}(M-1,z)\right]^T = \\ &\tfrac{\mathbf{W}^{*T}}{M^2}\left[A_0(z^{1/M}), A_1(z^{1/M}), \ldots, A_{M-1}(z^{1/M})\right]^T \qquad (4) \end{aligned}$$

where $\mathbf{W}^{*T}$ is the transjugated Fourier matrix, and $A_k(z)$ is the result of convolving the modulated DFT-spectra [11, 10]

$$A_k(z) = \sum_{l=0}^{M-1} T(zW^l)T(z^{-1}W^{k-l}) \quad (5)$$

The energy spectrum averaged over m then is

$$\overline{R}^E_{xx}(z) = \frac{1}{M^2} A_0(z^{1/M}) \quad (6)$$

and the shift-variant differences $\Delta R^E_{xx}(m,z) = R^E_{xx}(m,z) - \overline{R}^E_{xx}(z)$ to the average are

$$\left[\Delta R^E_{xx}(0,z), \ldots, \Delta R^E_{xx}(M-1,z)\right]^T = \frac{\mathbf{W}^{*T}}{M^2} \left[0, A_1(z^{1/M}), \ldots, A_{M-1}(z^{1/M})\right]^T . \quad (7)$$

The latter are zero if and only if $A_k(z) = 0$ for $k = 1, \ldots, M-1$, i.e., when no aliasing occurs.

2.1.2. WSS random signals

Decimation adds aliased components to the original power spectrum, but leaves the signal WSS. The power spectrum of the downsampled signal obeys

$$R_{xx}(z) = \frac{1}{M} \cdot \sum_{k=0}^{M-1} H(z^{-1/M}W^{-k}) \cdot R_{ss}(z^{1/M}W^k) H(z^{1/M}W^k) . \quad (8)$$

2.2. Interpolation

2.2.1. Deterministic signals

Interpolation of $x(n)$ causes no shift-variant behaviour, and results in

$$R^E_{yy}(z) = G(z) R^E_{xx}(z^M) G(z^{-1}) . \quad (9)$$

For the entire filter bank branch, we obtain by inserting Eq. (4)

$$\left[R^E_{yy}(0,z), \ldots, R^E_{yy}(M-1,z)\right]^T = \frac{\mathbf{W}^{*T}}{M^2} \left[B_0(z), \ldots, B_{M-1}(z)\right]^T \quad (10)$$

where

$$B_k(z) = G(z^{-1}) A_k(z) G(z) . \quad (11)$$

Thus, the average energy spectrum is

$$\overline{R}^E_{yy}(z) = \frac{1}{M^2} B_0(z) \quad (12)$$

and the shift-variant differences to the average after synthesis filtering are

$$\left[\Delta R^E_{yy}(0,z), \ldots, \Delta R^E_{yy}(M-1,z)\right]^T = \frac{\mathbf{W}^{*T}}{M^2} \left[0, B_1(z), \ldots, B_{M-1}(z)\right]^T . \quad (13)$$

2.2.2. WSS random signals

Upsampling and synthesis filtering generally causes a WSS signal to become wide-sense cyclostationary (WSCS) [6, 8]. In other words, the correlation structure depends periodically on the reference position m with period M. Arranging the power spectra $R_{yy}(m,z)$ for $m = 0, \ldots, M-1$ into a vector, we have shown in [12] that

$$\left[R_{yy}(0,z), \ldots, R_{yy}(M-1,z)\right]^T = \frac{R_{xx}(z^M)\mathbf{W}G(z)}{M} \mathbf{g}_m(z^{-1}) \quad (14)$$

holds. In [12], the derivation of this expression was based on a polyphase decomposition the interpolator, and formulating the sought cyclic nonstationary autocorrelation function of $y(n)$ in terms of cross correlation functions between the output signals of the polyphase components of $G(z)$. In the appendix, we provide here an alternative derivation using cyclic spectral density functions as defined in [7]. The average power spectrum is

$$\frac{1}{M} \sum_{i=0}^{M-1} R_{yy}(i,z) = \frac{R_{xx}(z^M)}{M} G(z) G(z^{-1}) . \quad (15)$$

In case of non-perfect anti-imaging filtering by $G(z)$, the nonstationary differences $\Delta R_{yy}(i,z)$ to the average spectrum are

$$\left[\Delta R_{yy}(0,z), \ldots, \Delta R_{yy}(M-1,z)\right]^T = \frac{R_{xx}(z^M)}{M} \cdot \mathbf{W}G(z) \left[0, G(z^{-1}W), \ldots, G(z^{-1}W^{M-1})\right]^T \quad (16)$$

These vanish for ideal anti-imaging filtering. To decribe the entire filter bank branch, we insert Eq. (8), yielding for the upsampled power spectrum $R_{xx}(z^M)$

$$R_{xx}(z^M) = \frac{1}{M} \cdot \sum_{k=0}^{M-1} H(z^{-1}W^{-k}) \cdot R_{ss}(zW^k) H(zW^k) . \quad (17)$$

3. QUANTIFYING SHIFT-VARIANT ENERGY

To assess shift variance of the energy at the output of the multirate filter bank branch, we integrate Eqs. (12) and (13) over the unit circle. With the aliasing component (AC) energy e_k

$$e_k = \frac{1}{2\pi M^2} \int_{-\pi}^{\pi} B_k(e^{j\omega}) d\omega \quad (18)$$

and invoking Parseval's theorem, we can relate the variance of the energy variation to the squared average energy given by $\overline{E}_{yy} = e_0$, and obtain

$$C^2_e(y) = \frac{\frac{1}{M}\sum_{m=0}^{M-1} |\Delta E_{yy}(m)|^2}{(\overline{E}_{yy})^2} = \frac{\sum_{k=1}^{M-1} |e_k|^2}{|e_0|^2} . \quad (19)$$

4. QUANTIFYING CYCLOSTATIONARY POWER

Similarly as above for deterministic signals, we can calculate the power of the WSCS output signal of the multirate filter bank branch by integrating over the unit circle. The generally periodically varying power $P_y(i)$ of the output signal $y(n)$ is

$$P_y(i) = \frac{1}{2\pi}\int_{-\pi}^{\pi} R_{yy}(i, e^{j\omega})d\omega\ , \quad i = 0, \ldots, M-1 \tag{20}$$

With p_n defined as

$$p_n = \frac{1}{2\pi M}\int_{-\pi}^{\pi} R_{xx}(e^{j\omega M})G(e^{j\omega})G(e^{-j(\omega+2\pi n/M)})d\omega \tag{21}$$

we obtain by integrating Eq. (14)

$$[P_y(0), \ldots, P_y(M-1)]^T = \mathbf{W}[p_0, \ldots p_{M-1}]^T \tag{22}$$

Thus, the average power $\overline{P}_y$ is

$$\overline{P}_y = \frac{1}{M}\sum_{i=0}^{M-1} P_y(i) = p_0 \tag{23}$$

and the deviations $\Delta P_y(i)$ from the average are

$$[\Delta P_y(0), \ldots, \Delta P_y(M-1)]^T = \mathbf{W}[0, p_1, \ldots, p_{M-1}]^T \tag{24}$$

To quantify the resulting cyclostationarity, we define the mean square power deviation from the average power as

$$C_p^2 = \frac{\frac{1}{M}\sum_{i=0}^{M-1}|\Delta P_y(i)|^2}{\left(\frac{1}{M}\sum_{i=0}^{M-1} P_y(i)\right)^2} = \frac{\sum_{n=1}^{M-1}|p_n|^2}{p_0^2} \tag{25}$$

These criteria - C_e^2 and C_p^2 - assess the shift variance of signal energy and the cyclic nonstationarity of the signal power, respectively. They can be applied to each subband of a critically sampled PR filter bank. Furthermore, via e_k and p_k, they provide information on which aliasing component is responsible for most of the variation. Changes in the energy spectra and power spectra, however, which do *not* result in a change of energy and power, respectively, are not captured by these criteria. For instance, shifting a deterministic impulse at the input of a filter bank channel with filters the coefficients of which are constant, such as the zeroth basis function of the DCT, would not result in a change of subband energy. Let us, however, additionally mention that, when applied to critically sampled orthogonal and biorthogonal filter banks, these criteria behave in a dual manner [11].

5. SHIFT-VARIANT ENERGY SPECTRA

For deterministic signals, changes in the energy spectra can be captured by interchanging the order of integration and applying Parseval's theorem, i.e., by first computing the squared modulus spectra $|B_k(e^{j\omega})|^2$. With

$$\begin{aligned}\sigma_e^2(\omega) &= \frac{1}{M}\sum_{m=0}^{M-1}|\Delta R_{yy}^E(m, e^{j\omega})|^2 \\ &= \frac{1}{M^4}\sum_{k=1}^{M-1}|B_k(e^{j\omega})|^2\end{aligned} \tag{26}$$

denoting the variance of the energy spectrum $R_{yy}^E(m, e^{j\omega})$ over m for each ω, a frequency-resolved measure of the variation of the energy spectrum can be obtained by the normalization

$$\begin{aligned}\sigma_{eN}^2(\omega) &= \frac{\sigma_e^2(\omega)}{|\overline{R}_{yy}^E(e^{j\omega})|^2} \\ &= \frac{\sum_{k=1}^{M-1}|B_k(e^{j\omega})|^2}{|B_0(e^{j\omega})|^2}\ .\end{aligned} \tag{27}$$

Averaging over ω yields the scalar measure

$$\begin{aligned}L_e^2 &= \frac{1}{2\pi}\int_{-\pi}^{\pi}\sigma_{eN}^2(\omega)d\omega \\ &= \frac{1}{2\pi}\int_{-\pi}^{\pi}\frac{\sum_{k=1}^{M-1}|B_k(e^{j\omega})|^2}{|B_0(e^{j\omega})|^2}d\omega\end{aligned} \tag{28}$$

Unlike the criterion C_e^2 above, this measure also captures changes in the energy spectra which do not result in a change of energy.

6. CYCLOSTATIONARY POWER SPECTRA

To capture also changes in power spectra which do not result in a change of signal power (and thus escape the above measure C_p^2), we first apply Parseval's theorem to Eq. (16), and integrate then over frequency, yielding

$$\sigma_p^2(m) = \frac{1}{2\pi}\int_{-\pi}^{\pi}|\Delta R_{yy}(m, e^{j\omega})|^2 d\omega \tag{29}$$

and

$$D_p^2(k) = \frac{1}{2\pi}\int_{-\pi}^{\pi}|C_k(e^{j\omega})|^2 d\omega \tag{30}$$

where

$$C_k(z) = \frac{R_{xx}(z^M)}{M}G(z)G(z^{-1}W^k) \tag{31}$$

With the mean-squared average spectrum

$$\mu_p^2 = \frac{1}{2\pi}\int_{-\pi}^{\pi}|\overline{R}_{yy}(e^{j\omega})|^2 d\omega \tag{32}$$

we get the normalized criterion

$$\begin{aligned}K_p^2 &= \frac{\frac{1}{M}\sum_{m=0}^{M-1}\sigma_p^2(m)}{\mu_p^2} \\ &= \frac{\sum_{k=1}^{M-1}D_p^2(k)}{D_p^2(0)}\end{aligned} \tag{33}$$

7. RESULTS

7.1. Deterministic signals

We first analyze the shift-variant behaviour of the energy spectra in orthogonal and biorthogonal two-channel filter banks and in 8-channel block transforms. The criterion employed is $L_e^2(i)$ defined in Eq. (28), which we evaluate for each subband signal. In addition, we show the normalized variance σ_{eN}^2 given in Eq. (27) over frequency

filter type	$L_e^2(0)$	$L_e^2(1)$	avg.
john-8	0.1973	0.4345	0.3159
john-16	0.1089	0.1892	0.1491
PR-CQF-8	0.0462	0.0748	0.0605
PR-CQF-16	0.0303	0.0395	0.0349
M-PR-QMF-8	0.2005	0.4445	0.3225
SHA03	0.2032	0.4501	0.3266
BIOR9/7	0	0	0
BIOR6/10	0.2122	0.3098	0.2610

Table 1. Values of $L_e^2(i)$ for subbands $i = 0$ and $i = 1$ of two-channel PR filter banks. The last column shows the average over both subbands.

for selected filter types. Results assessing the shift-variant behaviour of subband energy based on the measure C_e^2 in Eq. (19) were already given in [11]. Since the effects of shift variance in images are strongly visible at thin, line-like structures, our test signal $s(n)$ in all cases is a double impulse without sign change, i.e., two successive unit impulses. Calculations of L_e^2 are carried out using the DFT as described in [11]. The DFT length in all cases was $N = 128$, with the filter responses padded appropriately by zeros. The results are summarized in Table 1. The first two rows (john-8, john-16) refer to the Johnston filters of lengths 8 and 16, repectively. These are linear-phase quadrature mirror filters with approximate PR properties [13, 14]. The longer filters provide better band separation, and correspondingly lower shift variance. PR-CQF-8 and PR-CQF-16 refers to the PR-conjugated quadrature filters by Smith and Barnwell, which are not linear phase, but provide perfect reconstruction [15, 14]. As assessed by our criterion, they are considerably less shift-variant, with L_e^2 decreasing as the filter length increases. M-PR-QMF-8 denotes the multiplierless PR-quadrature mirror filters of length eight, which can be found in, e.g., [14] (coefficients: $[-8, 8, 64, 64, 8, -8, 1, 1]$). The filter denoted by SHA03 is the optimal shift-invariant wavelet in [16] of length 8 (coefficients: 0.0073, 0.015, -0.1197, 0.0698, 0.7196, 0.6711, 0.0999, -0.0488), which, with respect to L_e^2 and our test signal, appears to perform less well than, e.g., the PR-CQ-filter of the same length, and no better than the M-PR-QMF-8 filters. The last two rows evaluate the biorthogonal 9/7 wavelets, and the biorthogonal filter pair of lengths 6/10 found in [17] to have low shift variance (coefficients: 0.788486, 0.047699,-0.129078 and 0.615051, 0.133389, -0.067237, 0.006989, 0.018914; both biorthogonal pairs are linear-phase filters). Among these filters, the biorthogonal 9/7 filters performed best, with no measurable shift variance as evaluated by L_e^2.

Figures 2 and 3 show the normalized variance $\sigma_{eN}^2(\omega)$ over frequency ω from zero to 2π. These diagrams allow to identify the frequencies which contribute strongest to shift variance. For each of the two subbands, $\sigma_{eN}^2(\omega)$ was calculated according to Eq. (27), the figures show the averages. A comparison of the figures shows that for the

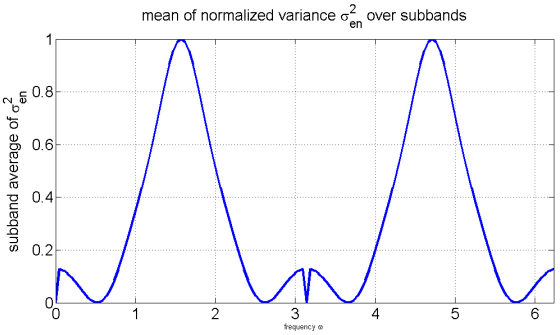

Figure 2. Normalized variance $\sigma_{eN}^2(\omega)$ averaged over both subbands for the Johnston filters of length 8, shown for $0 \leq \omega < 2\pi$.

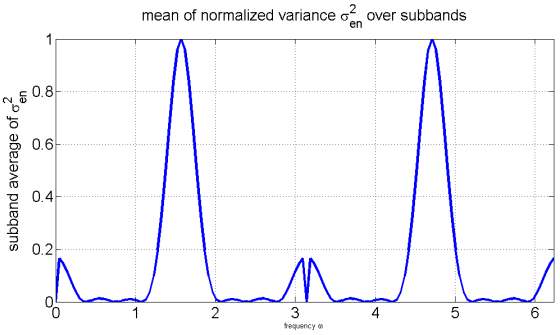

Figure 3. Normalized variance $\sigma_{eN}^2(\omega)$ averaged over both subbands for the Johnston filters of length 16, shown for $0 \leq \omega < 2\pi$.

longer filters, the effective bandwidth of the frequency intervals contributing to shift variance is lower.

Figures 4, 5 and 6 show the same results for the PRCQF-8, PRCQF-16 and multiplierless PR-QMF-8 filters.

Figures 7 and 8 depict these diagrams for the filter developed in [16] and the biorthogonal 6/10 pair.

To complement these measurements, Table 2 shows the results for a different input signal $s(n)$, viz. a double-sided deterministic signal the energy spectrum of which is identical to the power spectrum of a WSS AR(1)-process with correlation coefficient $\rho = 0.95$. The signal now extends over a much larger effective time interval than the above double impulse. For this lowpass-like signal, the Johnston-QM filters, the biorthogonal 6/10 pair and the multiplierless PR-QM filters perform best.

Results for the DCT, MLT and LOT, each for $M = 8$, and $s(n)$ again being the double impulse, can be found in Table 3. The length of the DCT basis functions correspondingly is 8, while both the MLT and the LOT basis functions have length 16. The LOT basis functions were computed for an AR(1)-process with correlation coefficient $\rho = 0.95$ as described in [18, 19]. As expected, the DCT is poorest, since its basis functions are only half as long as those of MLT and LOT, while the MLT leads the field. The normalized variances averaged over all subbands of each transform are given in Figs. 9, 10 and 11.

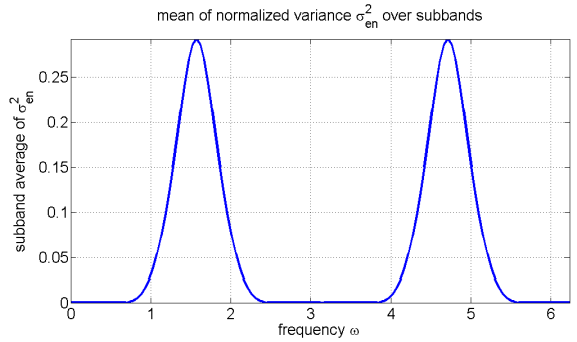

Figure 4. Normalized variance $\sigma^2_{eN}(\omega)$ averaged over both subbands for the PR-CQ filters of length 8, shown for $0 \leq \omega < 2\pi$.

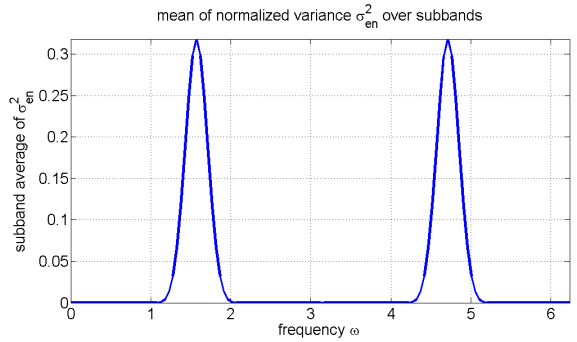

Figure 5. Normalized variance $\sigma^2_{eN}(\omega)$ averaged over both subbands for the PR-CQ filters of length 16, shown for $0 \leq \omega < 2\pi$.

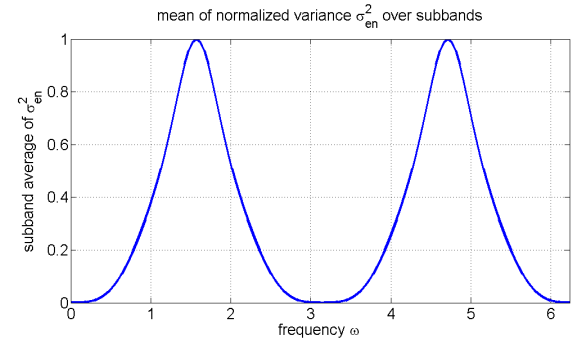

Figure 6. Normalized variance $\sigma^2_{eN}(\omega)$ averaged over both subbands for the multiplierless PR-QM filters of length 8, shown for $0 \leq \omega < 2\pi$.

filter type	$L^2_e(0)$	$L^2_e(1)$	avg.
john-8	0	0	0
john-16	0	0	0
PR-CQF-8	0.1245	0.2511	0.1878
PR-CQF-16	0.0736	0.1206	0.0971
M-PR-QMF-8	0.0038e-03	0.1812e-03	0.0925e-03
SHA03	0.0045	0.0313	0.0179
BIOR9/7	0.2206	0.3037	0.2621
BIOR6/10	0	0	0

Table 2. Values of $L^2_e(i)$ for subbands $i = 0$ and $i = 1$ of two-channel PR filter banks. The last column shows the average over both subbands. The test signal here is a double-sided expontial-like impulse the energy spectrum of which is equal to the power spectrum of a WSS AR(1) random signal.

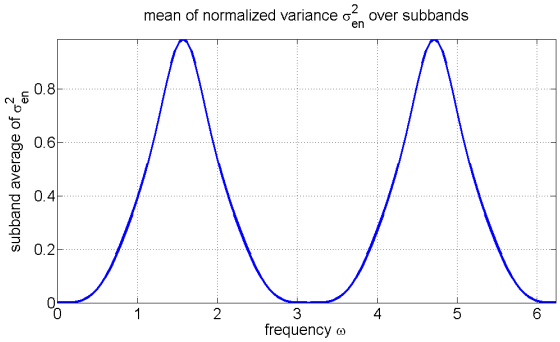

Figure 7. Normalized variance $\sigma^2_{eN}(\omega)$ averaged over both subbands for the optimized filter of length 8 from [16], shown for $0 \leq \omega < 2\pi$.

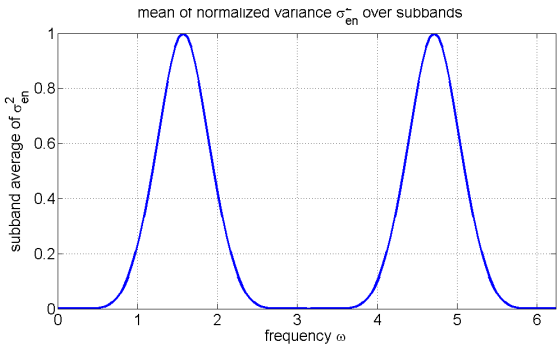

Figure 8. Normalized variance $\sigma^2_{eN}(\omega)$ averaged over both subbands for the biorthogonal 6/10 filter pair, shown for $0 \leq \omega < 2\pi$.

transform	$L^2_e(0)$	$L^2_e(1)$	$L^2_e(2)$	$L^2_e(3)$	$L^2_e(4)$
DCT	0.0512	0.5234	0.5295	0.5234	1.1796
MLT	0.1615	0.3279	0.3282	0.1846	0.1350
LOT	0.1778	0.3102	0.3726	0.5433	0.5876

	$L^2_e(5)$	$L^2_e(6)$	$L^2_e(7)$	avg.	
DCT	0.5234	0.5295	0.5234	0.5479	
MLT	0.3334	0.3457	0.5491	0.2957	
LOT	0.5672	0.3693	0.7316	0.4574	

Table 3. Shift variance measure for each subband of DCT, MLT, and LOT. The last column lists the averages.

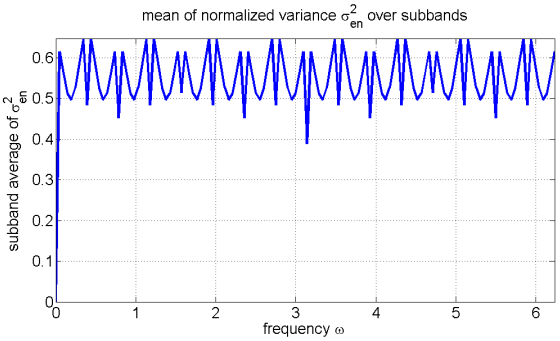

Figure 9. Normalized variance $\sigma^2_{eN}(\omega)$ averaged over the eight subbands for the DCT, shown for $0 \leq \omega < 2\pi$.

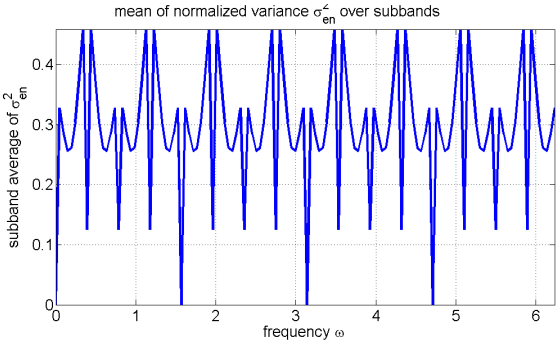

Figure 10. Normalized variance $\sigma^2_{eN}(\omega)$ averaged over the eight subbands for the MLT, shown for $0 \leq \omega < 2\pi$.

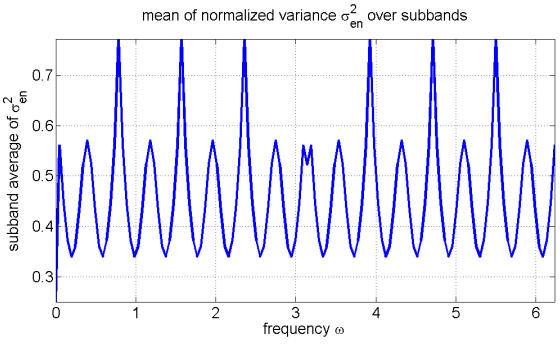

Figure 11. Normalized variance $\sigma^2_{eN}(\omega)$ averaged over the eight subbands for the LOT, shown for $0 \leq \omega < 2\pi$.

transform	$K_p^2(0)$	$K_p^2(1)$	$K_p^2(2)$	$K_p^2(3)$	$K_p^2(4)$
DCT	0.0179	1.3909	1.7700	1.7836	1.7822
MLT	0.0080	0.6967	0.7006	0.6995	0.6994
LOT	0.0115	0.7589	0.6828	0.7582	0.7077
	$K_p^2(5)$	$K_p^2(6)$	$K_p^2(7)$	avg.	
DCT	1.6960	1.4697	0.6820	1.3240	
MLT	0.6989	0.6968	0.2794	0.5599	
LOT	0.8673	0.7874	0.3691	0.6179	

Table 4. Measure for the cyclostationary behaviour of each subband of DCT, MLT, and LOT. The last column lists the averages.

7.2. Random signals

For random signals, we evaluated the cyclostationary behaviour of the power spectrum at the output of the filter bank branch by criterion $K_p^2(i)$ in Eq. (33) for each subband. The WSS test input signal $s(n)$ was a sample from an AR(1)-process with correlation coefficient $\rho = 0.95$. The results are shown in Table 4. As above, the DCT performs poorest, while the MLT performs best. Note that, when evaluating only the cyclostationary behaviour of the signal powers (rather than of the power *spectra*) by criterion C_p^2 in Eq. (25), the LOT performs better than the MLT (see [11]).

8. CONCLUSIONS

We have extended our earlier results on the evaluation of time-variant phenomena in multirate filter banks by new criteria, which do not only capture the changes in energy and power, but also assess changes in the shapes of energy spectra and power spectra. We have applied these to a variety of multirate filter banks. Clearly, the properties of the signals processed, in particular temporal extent and spectral content, have an influence on how critical these effects are. For shift variance of deterministic signals, we have therefore examined two different test signals, one being very short, which would correspond to the profile of a thin line in images, while the other is rather lowpass-like with larger temporal extent. In images, the profile of the latter would correspond to a wide ridge. Our framework and results could thus help in the selection of filters appropriate for a specific application, or with reasonably good behaviour over a variety of signals.

9. APPENDIX

To derive Eq. (14), we examine the cyclic correlation function which is defined in [7, Eq. (21)]. In our notation, the cyclic correlation function reads

$$r^c_{yy}(m,n) = \frac{1}{M} \sum_{k=0}^{M-1} r_{yy}(k,n) W^{-mk} \qquad (34)$$

Its transform with respect to n is the cyclic spectral density function $S_{yy}(m,z)$ [7, Eq. (22)] given by

$$\begin{aligned} S_{yy}(m,z) &= \sum_{n=-\infty}^{\infty} r_{yy}^{c}(m,n)z^{-n} \qquad (35) \\ &= \frac{1}{M}\sum_{k=0}^{M-1} W^{-mk} \sum_{n=-\infty}^{\infty} r_{yy}(k,n)z^{-n} \end{aligned}$$

With $\sum_n r_{yy}(k,n)z^{-n} = R_{yy}(k,z)$, the cyclic spectral density can be assembled into the vector

$$\begin{aligned} &[S_{yy}(0,z),\ldots,S_{yy}(M-1,z)]^T \quad = \\ &\frac{\mathbf{W}^{*T}}{M}[R_{yy}(0,z),\ldots,R_{yy}(M-1,z)]^T \qquad (36) \end{aligned}$$

Conversely, the vector with power spectra then is

$$\begin{aligned} &[R_{yy}(0,z),\ldots,R_{yy}(M-1,z)]^T \quad = \\ &\mathbf{W}[S_{yy}(0,z),\ldots,S_{yy}(M-1,z)]^T \qquad (37) \end{aligned}$$

With [7, Eq. (36)], the cyclic spectral density of the interpolated signal is

$$S_{yy}(m,z) = \frac{1}{M}G(z)R_{xx}(z^M)G(z^{-1}W^m) \qquad (38)$$

Inserting this into Eq. (37) leads to Eq. (14).

10. REFERENCES

[1] R. E. Crochiere and L. R. Rabiner, "Interpolation and decimation of digital signals – a tutorial review," *Proc. IEEE*, vol. 69, no. 3, pp. 300–331, 1981.

[2] R. E. Crochiere and L. R. Rabiner, *Multirate Digital Signal Processing*, Prentice-Hall, Englewood Cliffs, 1983.

[3] E. P. Simoncelli, W. T. Freeman, E. H. Adelson, and D. J. Heeger, "Shiftable multiscale transforms," *IEEE Transactions on Information Theory*, vol. 38, no. 2, pp. 587–607, 1992.

[4] C. M. Loeffler and C. S. Burrus, "Optimal design of periodically time-varying and multirate digital filters," *IEEE Transactions on Acoustics, Speech, and Signal Processing*, vol. 32, no. 5, pp. 991–997, 1984.

[5] F. Mintzer and B. Liu, "Aliasing error in the design of multirate filters," *IEEE Transactions on Acoustics, Speech, and Signal Processing*, vol. 26, pp. 76–88, 1978.

[6] V. P. Sathe and P. P. Vaidyanathan, "Effects of multirate systems on the statistical properties of random signals," *IEEE Transactions on Signal Processing*, vol. 41, no. 1, pp. 131–146, 1993.

[7] S. Ohno and H. Sakai, "Optimization of filter banks using cyclostationary spectral analysis," *IEEE Transactions on Signal Processing*, vol. 44, no. 11, pp. 2718–2725, 1996.

[8] S. Akkarakaran and P. P. Vaidynathan, "Bifrequency and bispectrum maps: A new look at multirate systems with stochastic inputs," *IEEE Transactions on Signal Processing*, vol. 48, no. 3, pp. 723–736, 2000.

[9] U. Petersohn, N. J. Fliege, and H. Unger, "Exact analysis of aliasing effects and non-stationary quantization noise in multirate systems," in *Proc. IEEE ICASSP*, Adelaide, May 1994, pp. III–173–III–176.

[10] T. Aach, "Shift variance and cyclostationarity in multirate filter banks," in *6th Nordic Signal Processing Symposium (NORSIG)*, Meripuisto, Espoo, June 9–11 2004, pp. 85–88, IEEE, ISBN: 951-22-7065-X (print), 951-22-7031-5 (CD-ROM).

[11] T. Aach, "Quantitative comparison of shift variance and cyclostationarity in multirate filter banks," in *International Workshop on Spectral Methods and Multirate Signal Processing (SMMSP)*, T. Saramäki, K. Egiazarian, and J. Astola, Eds., Vienna, Sept. 11 – 12 2004, pp. 7–14, TICSP Series, ISBN: 952-15-1229-6 (print), 952-15-1241-5 (CD-ROM).

[12] T. Aach, "Shift variance in multiscale filtering," in *International Workshop on Spectral Methods and Multirate Signal Processing (SMMSP)*, T. Saramäki, K. Egiazarian, and J. Astola, Eds., Barcelona, Spain, September 13–14 2003, pp. 23–30, TICSP Series, ISBN: 952-15-1062-5.

[13] J. D. Johnston, "A filter family designed for use in quadrature mirror filter banks," in *Proc. ICASSP 1980*, Piscataway, 1980, pp. 291–294, IEEE.

[14] A. N. Akansu and R. A. Haddad, *Multiresolution Signal Decomposition*, Academic Press, Boston, 2001.

[15] M. J. T. Smith and T. P. Barnwell III, "A procedure for designing exact reconstruction filter banks for tree-structured subband coders," in *Proc. International Conference on Acoustics, Speech, and Signal Processing (ICASSP)*, Piscataway, March 1984, pp. 27.1.1–27.1.4, IEEE.

[16] L. K. Shark and C. Yu, "Design of shift-invariant orthonormal wavelet filter banks via genetic algorithm," *Signal Processing*, vol. 83, pp. 2579–2591, 2003.

[17] J. D. Villasenor, B. Belzer, and J. Liao, "Wavelet filter evaluation for image compression," *IEEE Transactions on Image Processing*, vol. 4, no. 8, pp. 1053–1060, 1995.

[18] H. S. Malvar, *Signal Processing with Lapped Transforms*, Artech House, Norwood, MA, 1992.

[19] T. Aach, *Fourier, Block and Lapped Transforms*, Advances in Imaging and Electron Physics (Vol. 128), pp. 1–52, P. W. Hawkes (Ed.), Academic Press, San Diego, CA, 2003.